Random organic framework membranes with hierarchical channels for H_2 separation

Luan, Liping; Shi, Puxin; Wang, Zhi; Kapteijn, Freek; Liu, Xinlei

DOI
10.1016/j.memsci.2024.122420

Publication date
2024

Document Version
Final published version

Published in
Journal of Membrane Science

Journal of Membrane Science 694 (2024) 122420

Contents lists available at ScienceDirect

Journal of Membrane Science

journal homepage: www.elsevier.com/locate/memsci

Random organic framework membranes with hierarchical channels for H_2 separation

Liping Luan [a,b,1], Puxin Shi [a,b,1], Zhi Wang [a,b], Freek Kapteijn [c], Xinlei Liu [a,b,*]

[a] Chemical Engineering Research Center, School of Chemical Engineering and Technology, Tianjin University, Tianjin, 300072, China
[b] Tianjin Key Laboratory of Membrane Science and Desalination Technology, Haihe Laboratory of Sustainable Chemical Transformations, State Key Laboratory of Chemical Engineering, Tianjin University, Tianjin, 300072, China
[c] Catalysis Engineering, Department of Chemical Engineering, Delft University of Technology, 2629 HZ, Delft, the Netherlands

ARTICLE INFO

Keywords:
Random organic framework membranes
Benzimidazole and imine linked polymer
Hierarchical channels
H_2 separation

ABSTRACT

Novel membrane materials for H_2 separation are wanted. How to overcome the "trade-off" between membrane permeability and selectivity is a tough challenge. Here we report new random organic framework membranes with benzimidazole and imine linkages to form hierarchical channels. Both high H_2-selective and fast H_2 transport pathways are created. The preparation parameters are thoroughly studied and the membrane structures are well characterized by SEM, AFM, NMR, XPS, gas sorption, etc. Effect of feed conditions on membrane performance, such as composition, pressure and temperature, is investigated. The membrane performance transcends the upper bounds of H_2/CO_2, H_2/N_2 and H_2/CH_4 with excellent stability.

1. Introduction

Hydrogen is an ideal energy carrier since it is clean and sustainable [1,2]. Currently, the majority of H_2 is produced from fossil fuel *via* steam reforming and water-gas shift reaction [3,4], where CO_2 is generated simultaneously. So, the efficient separation of H_2 and CO_2 is of great importance for H_2 production and CO_2 capture. Besides, some industrial exhaust gas contains considerable proportions of H_2, and recovery of this H_2 (for instance from N_2 or CH_4) is highly desired [5–7].

Membrane technology has the advantages of environmental friendliness, low cost and small footprints [8–10], and has been used in gas separation. Polymeric membranes dominate the current market because of their low cost and good processibility [11,12]. Polysulfone (PS) and polyimide (PI) membranes have been commercialized for recovering H_2 from N_2 and CH_4 [13]. Since the H_2 molecule is smaller (kinetic diameter 0.29 nm) and lighter than CO_2 (kinetic diameter 0.33 nm), the diffusivity of H_2 in normal polymers is higher. As CO_2 is a Lewis acid, it has good affinity with normal polymers. Hence, construction of polymer membranes with high H_2/CO_2 separation performance is extremely challenging.

Polybenzimidazole (PBI) has dense structures and exhibits a moderate H_2/CO_2 selectivity [14]. Nevertheless, PBI membranes have the limitation of low permeability and poor processibility [15,16]. Benzimidazole-linked polymers (BILPs) are network polymers and they are a subfamily of porous organic frameworks (POFs) [17]. The hydrogen bonds and π-π interaction among the polymeric chains endow the BILP with a small interchain spacing, and thus a good selectivity for H_2/CO_2 separation [18]. However, the H_2 permeance was still moderate. The H_2 separation performance of PI could be boosted by cross-linking [19–22]. Despite its potential, PI has some weaknesses, such as a not tightly packing of the polymer chains, resulting in a low selectivity [21,23].

Quite a number of polymeric membranes suffer from the "trade-off" between gas permeability and selectivity [11,24,25], as expressed by the so-called 'Robeson upper bound' [25]. Novel materials were developed to overcome this "trade-off", including polymers of intrinsic microporosity(PIMs) [26] and POFs such as crystalline covalent organic frameworks (COFs) with imine linkages [27–29]. These new polymers have the merits of excellent thermochemical stability, diverse structure, multiple packing styles [29,30], adjustable degree of cross-linking and porosity [31,32]. However, the study of these membranes for H_2 separation is still under exploration.

In this work, a new class of POFs, i.e., random organic frameworks (ROFs) were developed. ROFs, stand for amorphous network polymers with different linkages. Specifically, ROF benzimidazole and imine linked polymer (BIILP) membranes were synthesized (Fig. 1). Relying on

* Corresponding author. Chemical Engineering Research Center, School of Chemical Engineering and Technology, Tianjin University, Tianjin, 300072, China.
E-mail address: xinlei_liu1@tju.edu.cn (X. Liu).
[1] These authors contributed equally to this work.

https://doi.org/10.1016/j.memsci.2024.122420
Received 16 November 2023; Received in revised form 26 December 2023; Accepted 3 January 2024
Available online 4 January 2024

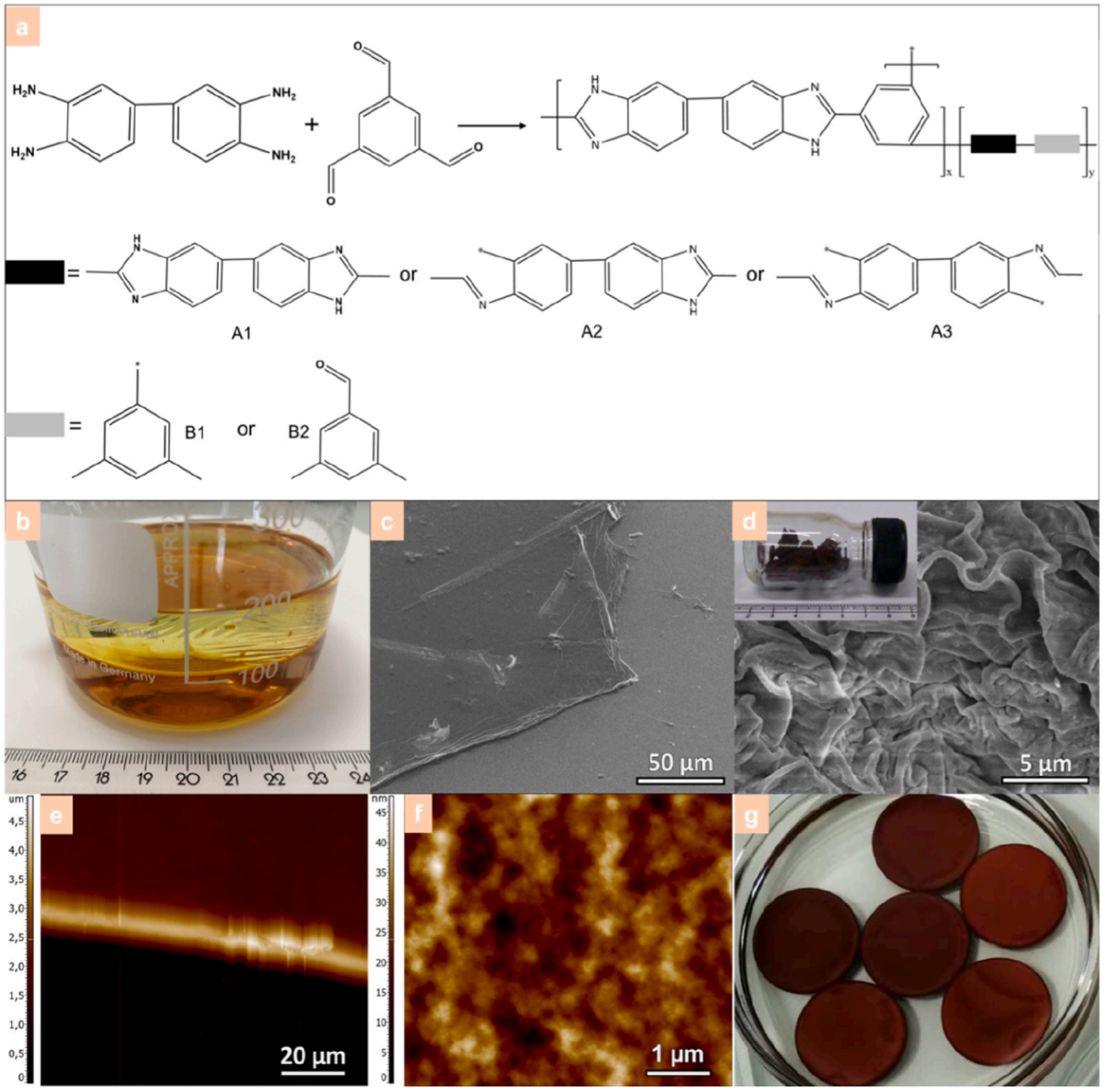

Fig. 1. Synthesis and morphology of BIILP films and membranes. (a) Chemical reaction equation for forming BIILP. (b) Photograph of a BIILP film formed between water and toluene phases in a beaker. (c) Surface SEM image of a BIILP film transferred to a silica wafer. (d) Surface SEM image of powdered BIILP films (The inset is a photograph of BIILP powdered films in a glass sample bottle). (e and f) AFM images of BIILP films transferred to a silica wafer. (g) Photograph of BIILP membranes formed on alumina disks (18 mm in diameter) between water and toluene phases in a petri dish. The film code for fig. b-f is F-1.5-0.50-120-298 and the membrane code for fig. g is M-1.5-0.50-120-298.

hydrogen bonding and π-π interaction between the polymeric chains, the packing of benzimidazole-linked segments is dense, providing narrow transient channels for H_2 to selectively pass through. When benzimidazole-linked segments were disrupted by imine segments, a relatively loose initial packing was created, and microporous channels were formed for fast H_2 transport. The combined synergistic effect of the hierarchical channels overcame the trade-off between permeability and selectivity. Consequently, the ROF BIILP membranes manifested excellent performance for separating H_2 from CO_2, N_2 and CH_4.

Table 1
Effect of feed temperature and pressure on membrane performance (M-1.5-0.50-120-298, feed conditions: single component gas.).

Temperature (K)	Pressure (bar)	P_{H2} (GPU)	P_{CO2} (GPU)	P_{N2} (GPU)	P_{CH4} (GPU)	α H_2/CO_2	α H_2/N_2	α H_2/CH_4
298	1	16.5	0.845	0.0910	0.234	19.5	181	70.6
323	1	31.9	1.30	0.130	0.286	24.5	245	111
348	1	57.5	2.46	0.221	0.364	23.4	260	158
373	1	82.6	3.60	0.325	0.455	22.9	254	181
	2	69.1	3.38	0.299	0.455	20.4	231	151
	3	60.1	3.20	0.325	0.468	18.8	185	129
	4	52.7	3.09	0.325	0.468	17.0	162	113

Table 2
H_2 separation performance of membranes synthesized under different conditions[a].

Membranes	H_2/CO_2		H_2/N_2		H_2/CH_4	
	P_{H2} (GPU)	$\alpha_{H2/CO2}$	P_{H2} (GPU)	$\alpha_{H2/N2}$	P_{H2} (GPU)	$\alpha_{H2/CH4}$
M-0.50-0.50-60-298	1660 ± 259	1.71 ± 0.58				
M-1.5-0.50-60-298	176 (408 ± 12)	18.2 (15.9 ± 1.1)				
M-3.0-0.50-60-298	194 ± 25	4.63 ± 0.12				
M-1.5-0.25-60-298	80.6 ± 5.5 (182)	10.9 ± 0.6 (11.2)				
M-1.5-1.0-60-298	322 ± 69 (451 ± 42)	6.17 ± 1.22 (7.62 ± 0.71)				
M-1.5-0.50-5.0-298	296 ± 21	8.14 ± 0.23				
M-1.5-0.50-120-298	107 ± 19 (171 ± 25)	24.4 ± 1.5 (20.7 ± 3.3)	83.6	317	93.2	189
M-1.5-0.50-180-298	84.5 ± 33.2	23.3 ± 0.8	113	224	110	163
M-1.5-0.0005-1440-298	176 ± 23	22.1 ± 1.4	189	301	201	261
M-1.5-0.05-2880-298	240 ± 66 (525 ± 112)	17.3 ± 0.6 (13.1 ± 3.3)	214 (440)	105 (108)	209 (421)	61.0 (76.0)
M-1.5-0.25-60-353	84.0 ± 8.1 (205)	14.2 ± 1.5 (9.9)				
M-1.5-0.5-60-353	268 ± 55 (670)	13.3 ± 1.4 (13.9)				

[a] Membrane codes: M-DAB concentration ($g{\cdot}mL^{-1} \times 100$)-TFB concentration ($g{\cdot}mL^{-1} \times 100$)-Reaction duration (min)-Reaction temperature (K). DAB: 3,3′ Diaminobenzidine, TFB: 1,3,5-triformylbenzene. Feed condition: 1 bar, 373 K (423 K in brackets), equimolar binary gas mixtures. Standard deviations of duplicate membranes are shown.

2. Methods

2.1. Preparation of supported membranes

Supported BIILP membranes were prepared by an interfacial polymerization protocol. A typical procedure is given here. 0.150 g 3,3′-diaminobenzidine tetrahydrochloride (DAB, ≥97.5 %, Sigma-Aldrich) and 0.0500 g 1,3,5-triformylbenzene (TFB, 97 %, Sigma-Aldrich) were dissolved in 10.0 mL homemade deionized water and 10.0 mL toluene (≥99 %, Sigma-Aldrich), respectively, with the assistance of ultrasonic. An α-Al_2O_3 disk (18.0 mm in diameter and 1.0 mm in thickness, Fraunhofer Institut für Keramische Technologien und Systeme, IKTS) with 10 μm-thick γ-Al_2O_3 top-layer which possesses smaller pore size (5 nm) and lower roughness, was immersed in the above DAB solution and then vacuum (0.20 bar, absolute pressure) was applied for 5 min to let the pores in the disk be filled with the solution. Afterwards, the disk was taken out from the solution and excessive aqueous droplets on the disk surface was removed by compressed air. To implement interfacial polymerization, the disk was immersed in TFB solution for 2 h at room temperature (298 ± 2 K) and left overnight under ambient conditions for drying. In the case of interfacial polymerization at 353 K (Table 2), disks containing DAB solutions were immersed in hot TFB solutions, preheated to 353 K in Teflon-lined autoclaves. 100 mL toluene was used when the concentration of TFB was lower than 0.1 ($g\ mL^{-1} \times 100$) (Table A2). The membranes prepared under different conditions were coded as M-DAB concentration ($g{\cdot}mL^{-1} \times 100$)-TFB concentration ($g{\cdot}mL^{-1} \times 100$)-Reaction duration (min)-Reaction temperature (K).

2.2. Preparation of powdered films

Powdered BIILP films were synthesized at bulk liquid interfaces. A typical procedure is given here. 1.50 g 3,3′-diaminobenzidine tetrahydrochloride (DAB, ≥97.5 %, Sigma-Aldrich) and 0.500 g 1,3,5-triformylbenzene (TFB, 97 %, Sigma-Aldrich) were dissolved in 100 ml homemade deionized water and 100 ml toluene (≥99 %, Sigma-Aldrich), respectively, with the assistance of ultrasonic. The TFB solution was then poured onto the DAB solution in a beaker. After 10 s vigorous stirring, the solution was sealed and left at room temperature (298 ± 2 K) for 2 h without disturbance. Afterwards, the powdered films were rinsed with toluene and water and dried under vacuum at 353 K. In case of powdered films, F was used to substitute M in the membrane codes.

2.3. Gas permeation testing

The obtained membranes were sealed in home-made Wicke-Kallenbach cells to evaluate their single component and mixed gas permeation performance. The pressure of sweep gas (Ar) was kept constant under ambient conditions. The setup was described elsewhere [17,33]. The feed temperature varied from 298 to 423 K, and the feed pressure in the range of 1-4 bar was employed. Gas permeance (P) and selectivity (α) are the two parameters to describe membrane permeation performance. The equation to calculate gas permeance of component i (P_i) reads as follows:

$$P_i = \frac{N_i}{\triangle p_i A}$$

The symbols are explained here: N_i, permeation rate ($mol{\cdot}s^{-1}$); ΔP_i, partial pressure difference (Pa); A, membrane area (m^2). Gas Permeation Unit (GPU) is widely reported as a unit of gas permeance, where 1 GPU $= 3.35 \times 10^{-10}$ mol s^{-1} $m^{-2}{\cdot}Pa^{-1}$. Permeability is a permeance multiplied by membrane thickness with a unit of Barrer (1 Barrer $= 3.35 \times 10^{-16}$ mol m $s^{-1}{\cdot}m^{-2}$ Pa^{-1}). In this work, membrane thickness (i.e., the thickness of separation layers) was quantified from cross-sectional SEM images. All the pressures used in this work are absolute pressures.

The gas selectivity is defined as the ratio of their permeance in the mixture (permselectivity):

$$\alpha_{i/j} = \frac{P_i}{P_j}$$

Ideal selectivity is calculated when single component gas permeation data are used.

At 423 K and 2 bar equimolar mixed gas conditions, the H_2 permeance of the bare substrates was >80,000 GPU with a low H_2/CO_2 selectivity of ~3.

2.4. Structural characterizations

Atomic force microscopy (AFM) tomography measurements were done in the tapping mode using a silicon tip (NSG03, NT-MDT), with a nominal value of the tip radius of 7 nm and a nominal spring constant of 0.4-2.7 N m^{-1} at a scan rate of 1 Hz under ambient conditions.

Photographs of BIILP membranes and films were made by a Huawei mobile phone (JKM-AL00b).

Scanning electron microscopy (SEM) images of BIILP membranes and films were acquired using a JEOL 6010 microscope. The specimens were gold-sputtered before analysis.

A Bruker-D8 Advance diffractometer (using Co $K\alpha$ radiation, λ = 0.179 nm at 40 mA and 35 kV) was employed to record the X-ray diffraction (XRD) patterns of BIILP films.

Diffuse reflectance infrared Fourier transform (DRIFT) spectra of BIILP films were acquired in a Nicolet 8700 FT-IR (Thermo Scientific) spectrometer. Before characterization, the samples were dried at 393 K under vacuum overnight.

^{13}C Cross-polarization Magic angle spinning (CP/MAS) solid state

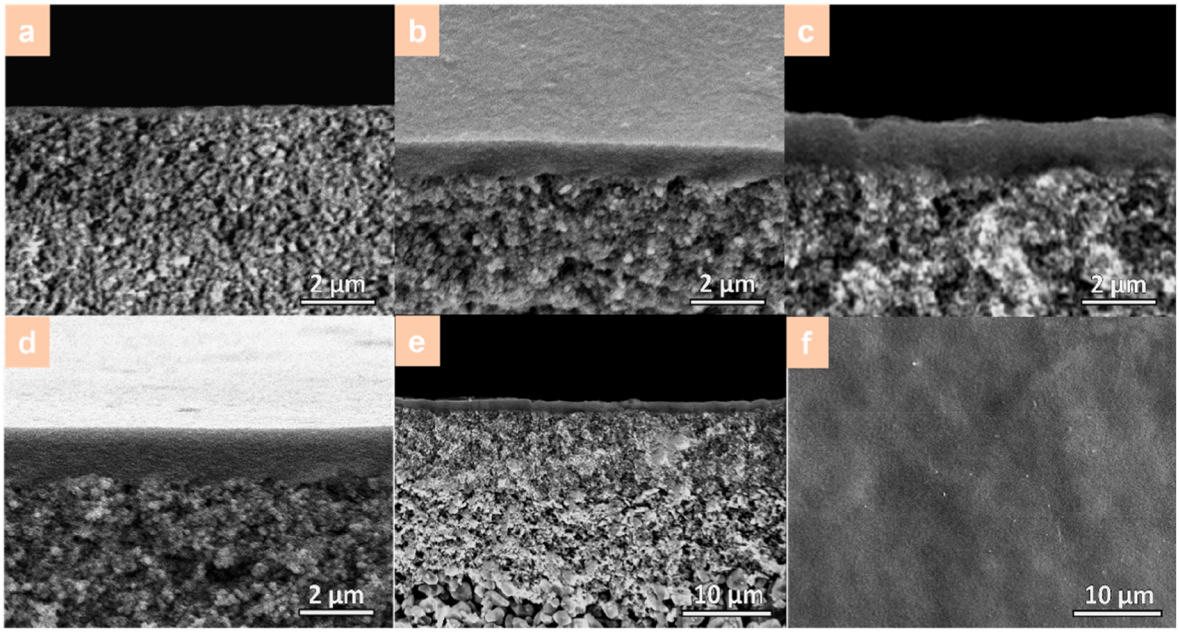

Fig. 2. SEM images of the membranes. (a, b, c and d) Cross-sectional SEM images of the membranes with different interfacial polymerization duration (5.0, 60, 120 and 180 min corresponding to M-1.5-0.50-5.0-298, M-1.5-0.50-60-298, M-1.5-0.50-120-298 and M-1.5-0.50-180-298, respectively.). (e and f) Cross section and surface SEM images of M-1.5-0.50-120-298 at lower magnification.

nuclear magnetic resonance (NMR) spectra of BIILP films were recorded using a Bruker Ascend 500 spectrometer, operating at a 125.76 MHz ^{13}C frequency, and equipped with a two channel 4 mm MAS probe head (Bruker) at a 10 kHz spinning speed. A proton $\pi/2$ pulse length of 3 μs, and a CP period of 2 ms was employed. 140000 scans were obtained, with a recycle delay of 5 s, in between scans. Prior to Fourier transformation, an exponential apodization function corresponding to a 80 Hz frequency line broadening was applied.

X-Ray photoelectron spectra (XPS) of a BIILP membrane (M-1.5-0.50-60-298) were obtained using a K-Alpha Thermo Fisher Scientific spectrometer equipped with Al- *Kα* X-ray source. To get depth profile images, the membrane was etched with a step length of 10 nm from surface to interior in a thickness range of 0-700 nm.

Thermogravimetic analysis (TGA) was used to qualify the thermal stability of the BIILP films in a temperature range of 303-1100 K using a Mettler Toledo TGA/SDTA851e apparatus, by measuring the loss in sample mass with an assigned heating rate of 5 K min^{-1}.

CO_2 (323 K) physisorption isotherms for BIILP films were obtained by employing the TriStar II 3020 (Micromeritics) instrument. Prior to adsorption tests, the powdered samples were dried at 393 K under a N_2 flow overnight.

3. Results and discussion

3.1. Synthesis and morphology

In general, the BIILP films and membranes were prepared by an interfacial polymerization (IP) protocol (see Fig. 1 and Methods section) [34]. Fig. 1(a) indicates the chemical reaction equation for forming BIILP using 3,3′-diaminobenzidine (DAB) and 1,3,5-triformylbenzene (TFB) monomers. When TFB toluene phase was poured onto DAB water phase, the polymerization took place and an orange film was clearly visible at the interface between the immiscible phases. The surface of the free-standing films was continuous and smooth although some particles were recognized in Fig. 1(c-f). The layers were uniform in micrometer thickness. The films prepared under different conditions were coded as F-DAB concentration ($g{\cdot}mL^{-1} \times 100$)-TFB concentration ($g{\cdot}mL^{-1} \times 100$)-Reaction duration (min)-Reaction temperature (K).

When alumina disks were placed between the two phases, supported BIILP membranes were directly formed in Figs. 1(g) and Fig. 2. (See

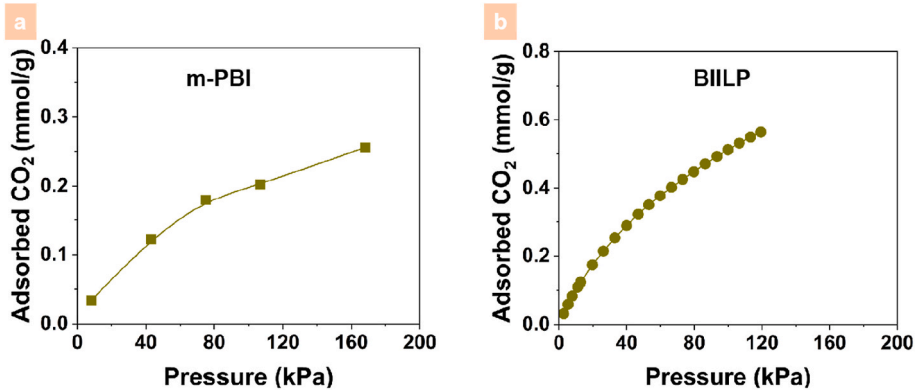

Fig. 3. Gas adsorption isotherms. (a-b) CO_2 adsorption isotherms of m-PBI (a) and BIILP (F-1.5-0.50-120-298) (b) at 323 K. The data in Fig. a were picked from our previous report [15].

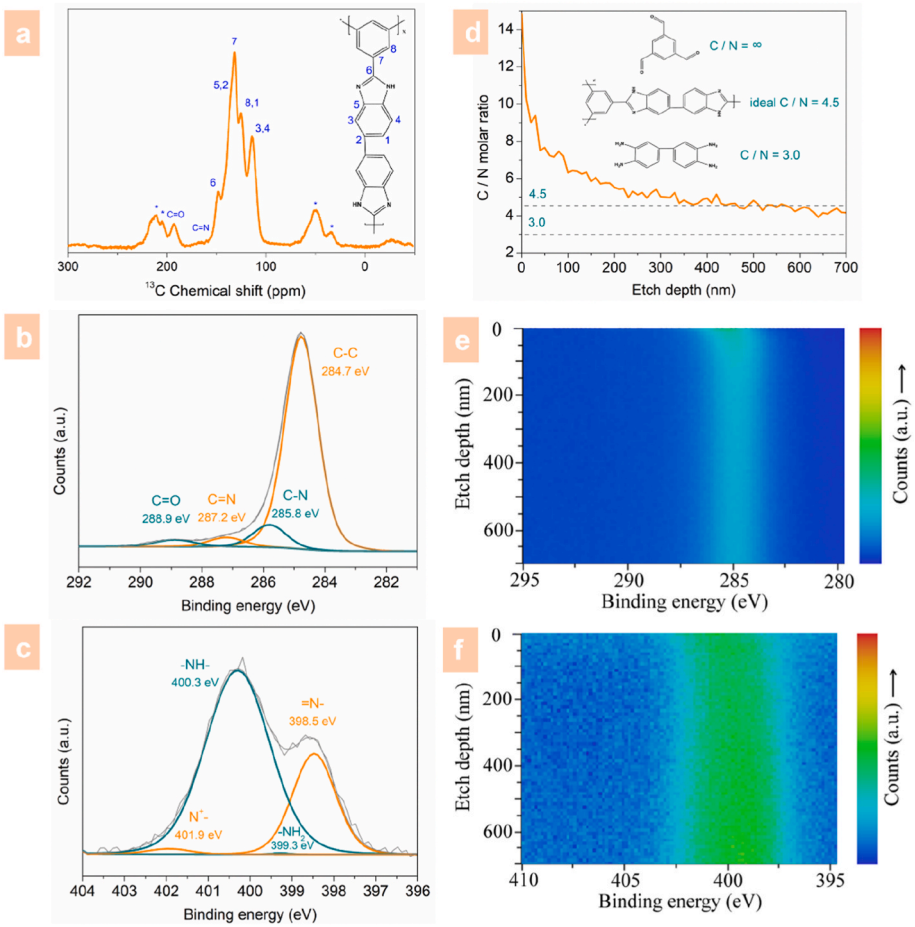

Fig. 4. Characterization of chemical structures. (a) ^{13}C solid-state NMR spectrum of BIILP films. (b and c) Deconvoluted C*1s* and N*1s* XPS spectra of a BIILP membrane. (d) C/N molar ratio profile with etch depth of a BIILP membrane calculated from XPS spectra. (e and f) Depth profile images of a BIILP membrane at C*1s* and N*1s* XPS regions. The specific film and membrane characterized in this figure are F-1.5-0.50-120-298 and M-1.5-0.50-60-298.

details of preparation in the Methods section). For membrane codes, M was used to substitute F in the film codes. The membrane thickness was around 0.15, 0.80, 1.30 and 1.40 μm corresponding to the IP duration of 5.0, 60, 120 and 180 min, respectively (Fig. 2). The membrane thickness increased gradually with IP duration since more monomers participated in the reaction. However, the rate of thickness increase dropped with IP duration due to the self-inhibition by the already-formed membrane layer, reducing the transport of monomers and the decrease of monomer concentration in the water phase. The morphology of the membrane surface was similar as the films.

3.2. Textural and chemical structures

The amorphous structure of BIILP films was confirmed by the XRD pattern in fig. A1(c). A *d*-spacing of 0.35 nm was calculated from the single broad diffraction peak centered at 30°. It is attributed to the parallel face-to-face packing of benzimidazole chains, which was also observed in the benchmark m-PBI [35].

The CO_2 adsorption isotherms of m-PBI and BIILP are shown in Fig. 3. They belong to type II adsorption according to IUPAC [36]. Although a certain amount of CO_2 was adsorbed in m-PBI, the uptake is far below that of porous benzimidazole-based polymers [37]. It is understandable since the polymer chains are closely packed in m-PBI. Compared with m-PBI, A sharp increase of CO_2 uptake was observed for BIILP. This points to the presence of more micropores in the latter, which can provide fast transport for small gases. Fortunately, the CO_2 loading in benzimidazole-based polymers will drop strongly at higher temperatures (*e.g.* 423 K) [15], leaving channels for weakly adsorbing gases like H_2 to pass through. The Micropores and densely-packed polymer chains (to generate transient pores) afford the claim of hierarchical channels in the membranes.

The random chemical structure of BIILP proposed in Fig. 1(a) was proved by the ^{13}C solid-state NMR, XPS and FTIR spectra (Fig. 4(a-c) and Fig. A1(a)). The formation of benzimidazole rings was verified by the peak number 6 with chemical shift at around 150 ppm. Residual aldehyde groups from TFB monomers and C═N from imine linkages were present at ~193 and 160 ppm, respectively. The same information was found in the deconvoluted XPS and FTIR spectra. In details: C–N (285.8 eV), C═N (287.2 eV) and C═O (288.9 eV) from C*1s* profile of XPS; =N- (398.5 eV) and -NH- (400.3 eV) from N*1s* profile of XPS; C═O (1701 cm^{-1}), C═N (1632 and 1616 cm^{-1}) and benzimidazole rings (1456, 1327 and 1230 cm^{-1}) from FTIR.

To investigate the chemical composition inside the membrane layers, XPS spectra were further collected assistant with etching technique in Fig. 4(d-f). A membrane (M-1.5-0.50-60-298) with a thickness around 800 nm of Fig. 2(b) was etched with a step length of 10 nm from surface to interior in a thickness range of 0-700 nm. The content of C decreased gradually with etch depth while that of N increased. As stated above, the DAB (containing N) water phase was soaked in the substrate, and the TFB (without N) toluene phase floated on it. It can be rationalized that there was a transport resistance for the monomers diffusing to the other phase. So, the content of TFB (DAB) dropped (enhanced) with etch depth. These indicate the inhomogeneous composition along the direction perpendicular to the membrane surface.

About the thermal stability of BIILP, as shown in Fig. A1(b), the TGA profile appears three steps of weight loss. Firstly, the weight loss before

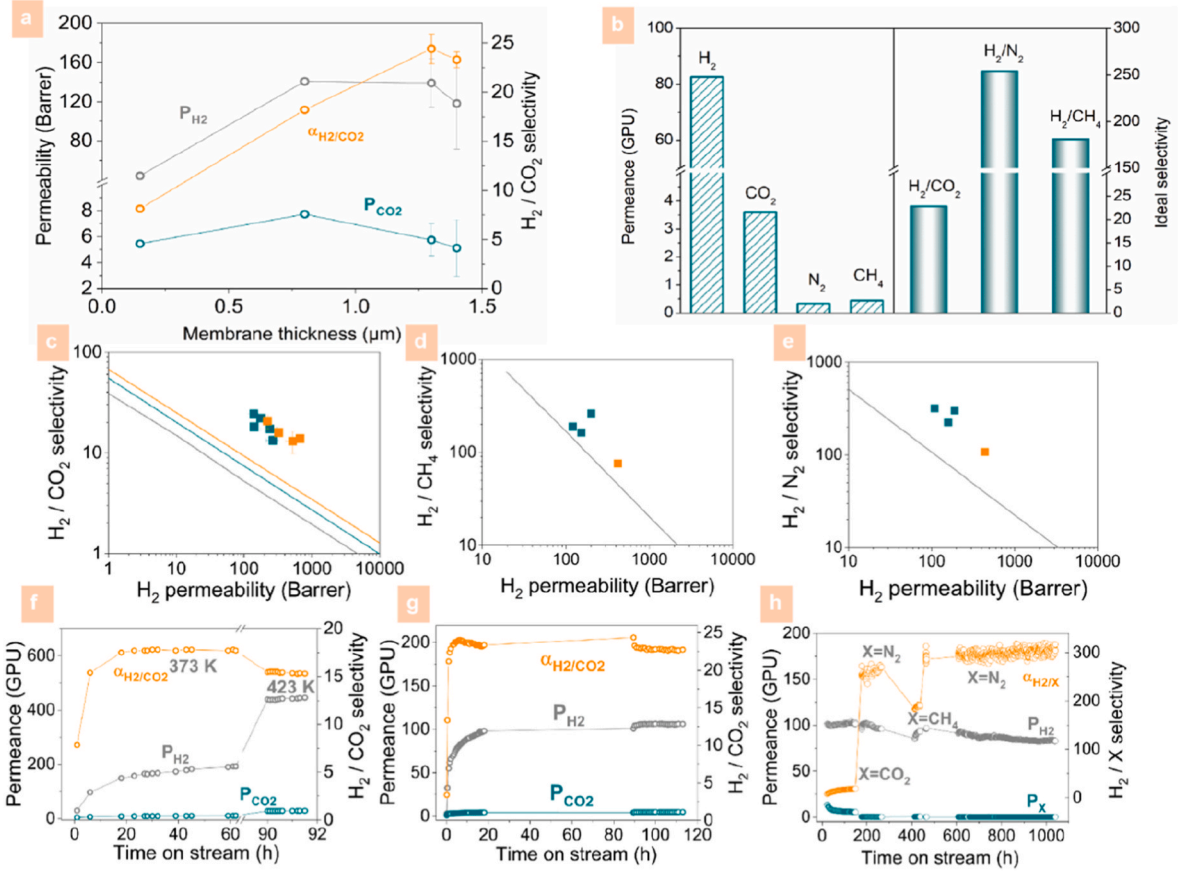

Fig. 5. BIILP membrane performance in H_2 separation. (a) Effect of membrane thickness on performance (M-1.5-0.50-5.0-298, M-1.5-0.50-60-298, M-1.5-0.50-120-298 and M-1.5-0.50-180-298. Feed conditions: 1 bar, 373 K, equimolar binary H_2/CO_2 gas mixture). (b) Single component gas permeance and ideal selectivity of a membrane (M-1.5-0.50-120-298. Feed conditions: 1 bar, 373 K). (c, d, and e) Membrane separation performance for H_2/CO_2, H_2/N_2, and H_2/CH_4 pairs (Feed conditions: 1 bar, 373 K (cyan squares) or 423 K (orange squares), equimolar binary gas mixtures. The data were transformed from Table 2. Robeson upper bound lines are shown for comparison: Grey, 308 K; cyan, 373 K; orange, 423 K.) [25,38]. The effect of temperature on the upper bound of H_2/CO_2 was calculated using activated diffusion model [38]. (f, g, and h) Effect of time on stream on membrane performance (f, M-1.5-0.05-2880-298. Feed conditions: 1 bar, equimolar binary H_2/CO_2 gas mixture. g, M-1.5-0.50-180-298. Feed conditions: 373K, 1 bar, equimolar binary H_2/CO_2 gas mixture. (h) M-1.5-0.50-120-298. Feed conditions: 1 bar, 373 K, equimolar binary gas mixture). Error bars are standard deviations of performance on basis of duplicated membranes. Lines are drawn to guide eyes. (For interpretation of the references to colour in this figure legend, the reader is referred to the Web version of this article.)

400 K was associated with physical desorption of excess solvent. The second stage between 500 and 600 K is a result of the escape of some residual monomers, which may be trapped within the layer confines of the backbone. The main frameworks started to decompose at around 750 K.

3.3. Membrane performance for H_2 separation

The H_2 separation performance (permeance and selectivity) is determined by the membrane structure, and the membrane structure is finally controlled by preparation conditions. With the extension of IP duration, the membrane thickness increased gradually (Fig. 2), and explains the decrease in H_2 permeance (Fig. A2(a)). The trends in gas permeability and selectivity in Fig. 5(a) indicate that structural evolution of membranes happened during IP. Residual monomers or oligomers might exist in the membrane layers at both short (5.0 min with a membrane thickness of ~0.15 μm) and long (180 min with a membrane thickness of ~1.40 μm) IP duration, partially blocking the channels for gas transport. Thus, lower permeability was observed. The IP duration of 60 min (membrane thickness of ~0.80 μm) and 120 min (membrane thickness of ~1.30 μm) could well balance gas permeance (and permeability) and selectivity as the membrane structure was well evolved. The effect of IP duration, monomer concentration and IP temperature was systematically studied. The membrane performance is shown in Fig. A2 and Table 2.

The single component permeation performance of H_2, CO_2, N_2 and CH_4 was conducted on the M-1.5-0.50-120-298. The results are illustrated in Fig. 5(b) and Table 1. The H_2 permeance (82.6 GPU) is far greater than that of the other gases. The gas permeance roughly dropped with their kinetic diameters (0.29, 0.33, 0.36 and 0.38 nm for H_2, CO_2, N_2 and CH_4, respectively.), suggesting a mechanism of size-dependent diffusion of the ROF BIILP membranes. The membrane achieved ideal selectivity of 22.9, 254, and 181 for H_2/CO_2, H_2/N_2 and H_2/CH_4 respectively. Interestingly, the H_2/CH_4 selectivity was lower than that of H_2/N_2. This phenomenon can be interpretated by the preferential adsorption of CH_4 in the BIILP.

The effect of feed temperature and pressure on the performance of M-1.5-0.50-120-298 was studied. As illustrated in Fig. 6(a)-c, the gas permeance increased with temperature, indicating that activated diffusion played an important role in gas transport. It is worth noting that the selectivity firstly increased and then remained steady. The permeance of H_2 and the selectivity decreased with feed pressure. The gas possibly followed the dual-sorption model since micropores were available in the BIILP (Fig. 3(b)). However, the uptakes were probably in their linear regions [15], because the membranes were evaluated at a relative high temperature (373 K) and a moderate pressure (total pressure up to 4.0 bar). The performance variation with pressure was largely due to the compression of polymer chains, which narrowed the effective pathways

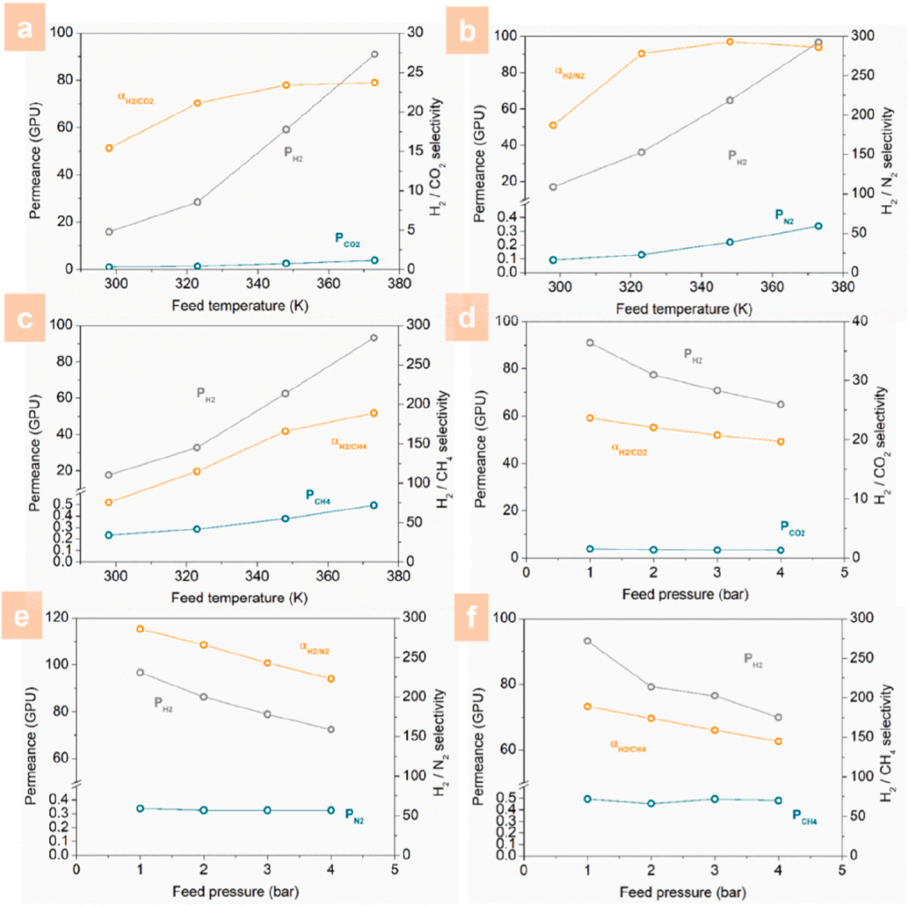

Fig. 6. Effect of feed temperature on the membrane performance for a 1 bar equimolar binary H_2/CO_2 (a), H_2/N_2 (b), and H_2/CH_4 (c); Effect of feed pressure on the membrane performance at 373 K for an equimolar binary feed of H_2/CO_2 (d), H_2/N_2 (e), and H_2/CH_4 (f), respectively (M-1.5-0.50-120-298).

of H_2.

In order to benchmark the BIILP membranes, their H_2 separation performance was compared with typical polymeric membranes. For instance, as listed in Table 2 and Table A1, the permeance of H_2 and the H_2/CO_2 selectivity reached 176 GPU and 22.1, respectively, surpassing that of most PBI (Table A2) and PI [39] membranes. The selectivity for H_2/N_2 and H_2/CH_4 was 301 and 261, respectively, with a H_2 permeance around 200 GPU, higher than previous polymeric membranes [40,41]. Furthermore, the membrane permeability, which reflects the nature of membrane materials, was calculated and compared with the Robeson upper bounds in Fig. 5(c-e). Typically, the H_2 permeability was around 200 Barrer. All the data surpassed the Robeson upper bounds. It validated the proposed synergistic effect of the hierarchical channels to overcome the "trade-off" between permeability and selectivity. Although imide linkages were possibly present in previous BILP membranes [17], the ROF BIILP membranes prepared in this work could better balance gas permeability and selectivity.

Membrane stability is very important for industrial applications. BIILP membranes (M-1.5-0.05-2880-298, M-1.5-0.50-180-298 and M-1.5-0.50-120-298) prepared under different conditions were evaluated with time on stream in Fig. 5(f-h). As the as-synthesized membranes were stored under ambient conditions, environment moisture was possibly adsorbed in the membrane channels. So, it took some time for the initial activation before steady state was reached. The membrane, as shown in Fig. 5(h), exhibited a stable performance for >1000 h, even in different gas mixtures. Only a small decrease in H_2 permeance and small increase in selectivity were observed, probably because of the closer packing of polymer chains.

4. Conclusion

In conclusion, new random organic framework (ROF) benzimidazole and imine linked polymer (BIILP) membranes were developed by interfacial polymerization (IP) strategy. The dense packing of benzimidazole-linked segments provided narrow and transient channels for H_2 to selectively pass through. When benzimidazole-linked segments were disrupted by imine segments, microporous channels were formed for fast H_2 transport. The synergistic effect of the hierarchical channels endowed the membranes with excellent performance for H_2/CO_2, H_2/N_2 and H_2/CH_4 separation and overcame the trade-off between permeability and selectivity.

CRediT authorship contribution statement

Liping Luan: Investigation, Methodology, Writing – original draft. **Puxin Shi:** Investigation, Methodology, Writing – original draft. **Zhi Wang:** Writing – review & editing. **Freek Kapteijn:** Writing – review & editing. **Xinlei Liu:** Funding acquisition, Investigation, Resources, Writing – review & editing.

Declaration of competing interest

The authors declare that they have no known competing financial interests or personal relationships that could have appeared to influence the work reported in this paper.

Data availability

The data that has been used is confidential.

Acknowledgements

This work was financially supported by the National Key Research and Development Program (2021YFB3801200), the National Natural Science Foundation of China (22008171), the Inner Mongolia Autonomous Region Unveiling Project (2022JBGS0027), and the Independent Innovation Funding of Tianjin University (No. 2023XJD-0067). The authors were grateful to Dr. D. Osadchii from TUDelft for his valuable discussion.

Appendix A. Supplementary data

Supplementary data to this article can be found online at https://doi.org/10.1016/j.memsci.2024.122420.

References

[1] W. Lubitz, W. Tumas, Hydrogen: an overview, Chem. Rev. 107 (2007) 3900–3903.
[2] G.I. Peterson, S. Yang, T. Choi, Polymers producing hydrogen, Nat. Chem. 12 (2020) 1093–1095.
[3] J.A. Turner, Sustainable hydrogen production, Science 305 (2004) 972–974.
[4] D. Mendes, A. Mendes, L.M. Madeira, A. Iulianelli, J.M. Sousa, A. Basile, The water-gas shift reaction: from conventional catalytic systems to Pd-based membrane reactors-a review, Asia-Pac, J. Chem. Eng. 5 (2010) 111–137.
[5] Y. Zhou, Y. Wu, H. Wu, J. Xue, L. Ding, R. Wang, H. Wang, Fast hydrogen purification through graphitic carbon nitride nanosheet membranes, Nat. Commun. 13 (2022) 5852.
[6] C. Shen, H. Qiu, W. Guo, Ultrahigh hydrogen and nitrogen selectivity achieved by the nanoporous graphene with a precise nanopore, Carbon 182 (2021) 628–633.
[7] W. Lin, J. Xu, L. Zhang, A. Gu, Synthetic natural gas (SNG) liquefaction processes with hydrogen separation, Int. J. Hydrogen Energy 42 (2017) 18417–18424.
[8] Z. Kang, S. Wang, L. Fan, M. Zhang, W. Kang, J. Pang, X. Du, H. Guo, R. Wang, D. Sun, In situ generation of intercalated membranes for efficient gas separation, Commun. Chem. 1 (2018) 3.
[9] Y. Cheng, S.J. Datta, S. Zhou, J. Jia, O. Shekhah, M. Eddaoudi, Advances in metal-organic framework-based membranes, Chem. Soc. Rev. 51 (2022) 8300–8350.
[10] Y. Liu, H. Liu, Z. Shen, Nanocellulose based filtration membrane in industrial waste water treatment: a review, Materials 14 (2021) 5398.
[11] H.B. Park, J. Kamcev, L.M. Robeson, M. Elimelech, B.D. Freeman, Maximizing the right stuff: the trade-off between membrane permeability and selectivity, Science 356 (2017) eaab530.
[12] Z. Qiao, S. Chai, K. Nelson, Z. Bi, J. Chen, S.M. Mahurin, X. Zhu, S. Dai, Polymeric molecular sieve membranes via in situ cross-linking of non-porous polymer membrane templates, Nat. Commun. 5 (2014) 3705.
[13] P. Bernardo, E. Drioli, G. Golemme, Membrane gas separation: a review/state of the art, Ind. Eng. Chem. Res. 48 (2009) 4638–4663.
[14] S.C. Kumbharkar, Y. Liu, K. Li, High performance polybenzimidazole based asymmetric hollow fibre membranes for H_2/CO_2 separation, J. Membr. Sci. 375 (2011) 231–240.
[15] M. Etxeberria-Benavides, T. Johnson, S. Cao, B. Zornoza, J. Coronas, J. Sanchez-Lainez, A. Sabetghadam, X. Liu, E. Andres-Garcia, F. Kapteijn, J. Gascon, O. David, PBI mixed matrix hollow fiber membrane: influence of ZIF-8 filler over H_2/CO_2 separation performance at high temperature and pressure, Sep. Purif. Technol. 237 (2020) 116347.
[16] J. Sánchez-Laínez, B. Zornoza, S. Friebe, J. Caro, S. Cao, A. Sabetghadam, B. Seoane, J. Gascon, F. Kapteijn, C. Le Guillouzer, G. Clet, M. Daturi, C. Téllez, J. Coronas, Influence of ZIF-8 particle size in the performance of polybenzimidazole mixed matrix membranes for pre-combustion CO_2 capture and its validation through interlaboratory test, J. Membr. Sci. 515 (2016) 45–53.
[17] M. Shan, X. Liu, X. Wang, I. Yarulina, B. Seoane, F. Kapteijn, J. Gascon, Facile manufacture of porous organic framework membranes for precombustion CO_2 capture, Sci. Adv. 4 (2018) eaau1698.
[18] S. Cong, J. Wang, Z. Wang, X. Liu, Polybenzimidazole (PBI) and benzimidazole-linked polymer (BILP) membranes, Green Chem. Eng. 2 (2021) 44–56.
[19] S. Wu, J. Liang, Y. Shi, M. Huang, X. Bi, Z. Wang, J. Jin, Design of interchain hydrogen bond in polyimide membrane for improved gas selectivity and membrane stability, J. Membr. Sci. 618 (2021) 118659.
[20] I. Hossain, A.Z. Al Munsur, O. Choi, T. Kim, Bisimidazolium PEG-mediated crosslinked 6FDA-durene polyimide membranes for CO_2 separation, Sep. Purif. Technol. 224 (2019) 180–188.
[21] L. Ansaloni, E. Louradour, F. Radmanesh, H. van Veen, M. Pilz, C. Simon, N. E. Benes, T.A. Peters, Upscaling polyPOSS-imide membranes for high temperature H_2 upgrading, J. Membr. Sci. 620 (2021) 118875.
[22] C. Ma, C. Zhang, Y. Labreche, S. Fu, L. Liu, W.J. Koros, Thin-skinned intrinsically defect-free asymmetric mono-esterified hollow fiber precursors for crosslinkable polyimide gas separation membranes, J. Membr. Sci. 493 (2015) 252–262.
[23] M.J.T. Raaijmakers, M.A. Hempenius, P.M. Schön, G.J. Vancso, A. Nijmeijer, M. Wessling, N.E. Benes, Sieving of hot gases by hyper-cross-linked nanoscale-hybrid membranes, J. Am. Chem. Soc. 136 (2014) 330–335.
[24] B.W. Rowe, L.M. Robeson, B.D. Freeman, D.R. Paul, Influence of temperature on the upper bound: theoretical considerations and comparison with experimental results, J. Membr. Sci. 360 (2010) 58–69.
[25] L.M. Robeson, The upper bound revisited, J. Membr. Sci. 320 (2008) 390–400.
[26] X. Chen, Y. Fan, L. Wu, L. Zhang, D. Guan, C. Ma, N. Li, Ultra-selective molecular-sieving gas separation membranes enabled by multi-covalent-crosslinking of microporous polymer blends, Nat. Commun. 12 (2021) 6140.
[27] H. Fan, M. Peng, I. Strauss, A. Mundstock, H. Meng, J. Caro, MOF-in-COF molecular sieving membrane for selective hydrogen separation, Nat. Commun. 12 (2021) 38.
[28] H. Fan, A. Mundstock, J. Gu, H. Meng, J. Caro, An azine-linked covalent organic framework ACOF-1 membrane for highly selective CO_2/CH_4 separation, J. Mater. Chem. A 6 (2018) 16849–16853.
[29] H. Fan, M. Peng, I. Strauss, A. Mundstock, H. Meng, J. Caro, Two-dimensional covalent triazine framework membrane for helium separation and hydrogen purification, J. Am. Chem. Soc. 142 (2020) 6872–6877.
[30] Y. Wang, J. Li, Q. Yang, C. Zhong, Two-dimensional covalent triazine framework membrane for helium separation and hydrogen purification, ACS Appl. Mater. Interfaces 8 (2016) 8694–8701.
[31] J. Lu, J. Zhang, Facile synthesis of azo-linked porous organic frameworks via reductive homocoupling for selective CO_2 capture, J. Mater. Chem. A 2 (2014) 13831–13834.
[32] M.G. Rabbani, T.E. Reich, R.M. Kassab, K.T. Jackson, H.M. El-Kaderi, High CO_2 uptake and selectivity by triptycene-derived benzimidazole-linked polymers, Chem. Commun. 48 (2012) 1141–1143.
[33] T. Rodenas, I. Luz, G. Prieto, B. Seoane, H. Miro, A. Corma, F. Kapteijn, F.X. Llabrés I Xamena, J. Gascon, Metal-organic framework nanosheets in polymer composite materials for gas separation, Nat. Mater. 14 (2015) 48–55.
[34] X. Wang, M. Shan, X. Liu, M. Wang, C.M. Doherty, D. Osadchii, F. Kapteijn, High-performance polybenzimidazole membranes for helium extraction from natural gas, ACS Appl. Mater. Interfaces 11 (2019) 20098–20103.
[35] K.Y. Wang, M. Weber, T. Chung, Polybenzimidazoles (PBIs) and state-of-the-art PBI hollow fiber membranes for water, organic solvent and gas separations: a review, J. Mater. Chem. A 10 (2022) 8687–8718.
[36] M. Thommes, K. Kaneko, A.V. Neimark, J.P. Olivier, F. Rodriguez-Reinoso, J. Rouquerol, K.S.W. Sing, Physisorption of gases, with special reference to the evaluation of surface area and pore size distribution (IUPAC Technical Report), Pure Appl. Chem. 87 (2015) 1051–1069.
[37] M. Shan, B. Seoane, A. Pustovarenko, X. Wang, X. Liu, I. Yarulina, E. Abou-Hamad, F. Kapteijn, J. Gascon, Benzimidazole linked polymers (BILPs) in mixed-matrix membranes: influence of filler porosity on the CO_2/N_2 separation performance, J. Membr. Sci. 566 (2018) 213–222.
[38] L. Hu, S. Pal, H. Nguyen, V. Bui, H. Lin, Molecularly engineering polymeric membranes for H_2/CO_2 separation at 100-300 °C, J. Polym. Sci. 58 (2020) 2467–2481.
[39] M.J.T. Raaijmakers, M. Wessling, A. Nijmeijer, N.E. Benes, Hybrid polyhedral oligomeric silsesquioxanes-imides with tailored intercage spacing for sieving of hot gases, Chem. Mater. 26 (2014) 3660–3664.
[40] P. Shao, R. Yao, G. Li, M. Zhang, S. Yuan, X. Wang, Y. Zhu, X. Zhang, L. Zhang, X. Feng, B. Wang, Molecular-sieving membrane by partitioning the channels in ultrafiltration membrane by in situ polymerization, Angew. Chem. Int. Ed. 59 (2020) 4401–4405.
[41] G.V. Sarrigani, J. Ding, A.E. Ghadi, D. Alam, P. Fitzgerald, D.E. Wiley, D.K. Wang, Interfacially-confined polyetherimide tubular membranes for H_2, CO_2 and N_2 separations, J. Membr. Sci. 655 (2022) 120596.